Ke Ai
ADVANCING RESEARCH
EVOLVING SCIENCE

Available online at www.sciencedirect.com

ScienceDirect

Journal of Natural Gas Geoscience 1 (2016) 243−249

http://www.keaipublishing.com/jnggs

Original research paper

The influence of soluble organic matter on shale reservoir characterization☆

Lei Pan [a,b], Xianming Xiao [a,*], Qin Zhou [a]

[a] State Key Laboratory of Organic Geochemistry, Guangzhou Institute of Geochemistry, Chinese Academy of Sciences, Guangzhou 510640, China
[b] Ocean College of Qinzhou University, Qinzhou 535000, China

Received 10 May 2016; revised 18 June 2016
Available online 3 August 2016

Abstract

Shale with a maturity within the "oil window" contains a certain amount of residual soluble organic matter (SOM). This SOM have an important influence on characterization of shale reservoir. In this study, two shale samples were collected from the Upper Permian Dalong Formation in the northwestern boundary of Sichuan Basin. Their geochemistry, mineral composition, and pore structure (surface area and pore volume) were investigated before and after removing the SOM by means of extraction via dichloromethane or trichloromethane. The results show that the TOC, S_1, S_2, and I_H of the extracted samples decrease significantly, but the mineral composition has no evident change as compared with their raw samples. Thus, we can infer that the original pore structure is thought to be unaffected from the extraction. The SOM occupies pore volume and hinders pores connectivity. The extraction greatly increases the surface area and pore volume of the samples. The residual SOM in the shale samples occur mainly in the micropores and smaller mesopores, and their occupied pore size range seems being constrained by the maturity. For the lower mature shale samples, the SOM is mainly hosted in organic pores that are less than 5 nm in size. For the middle mature shale samples, the micropores and some mesopores ranging between 2 and 20 nm in size are the main storage space for the SOM.

Keywords: Soluble organic matter; Shale oil and gas; Reservoir characteristic; Pore structure

1. Introduction

Most of the North American shales are in the middle and high mature stage ($1.2\% < R_O < 2.5\%$) [1−3]. Shales from various strata with various maturity levels are distributed extensively in China. The Lower Paleozoic shales in South China have relatively high maturity with EqR_O (equivalent vitrinite reflectance) value ranging from 2.0% to 4.0% [4−9]. The Upper Paleozoic shales are mainly in the middle and high mature stage ($1.5\% < R_O < 2.5\%$) [10−12], but some shales are still in relatively low mature stage ($R_O < 1.0\%$) [12,13]. The Lower Paleozoic shales in and around the Sichuan Basin were the focus of investigations and explorations in recent years [5−9], but the studies about reservoir properties in the Upper Paleozoic shales are comparatively few, especially shales with lower maturity. The studies about low mature coal have indicated that the SOM not only occupies a portion of porosity [14], but also has an important influence on methane adsorption [15]. The Soxhlet-extraction with dissimilar organic solvents have different product from shale [16], not to mention, the transformation of reservoir is also different [17]. The type and content of organic matter and the maturity of shale are the main factors in controlling pore structure [8,9,12,18−22]. The organic matter in shale is mainly composed of soluble organic matter and kerogen. For high mature shale, gas was generated and pyrobitumen formed by

☆ This is English translational work of an article originally published in *Natural Gas Geoscience* (in Chinese).The original article can be found at:10.11764/j.issn.1672-1926.2015.09.1719.

* Corresponding author.
E-mail address: xmxiao@gig.ac.cn (X. Xiao).

Peer review under responsibility of Editorial Office of *Journal of Natural Gas Geoscience*.

http://dx.doi.org/10.1016/j.jnggs.2016.07.004

cracking the heavy hydrocarbons and light hydrocarbons in the maturation process [18,19]. Shale with a maturity within "oil window" contains a certain amount of residual SOM. The amount of SOM for the type I-IIa shales can reach 20%–30% of total organic matter in the peak period of hydrocarbon generation. The SOM has apparent influence on the quantitative characterization of shale reservoir [12,18] that calls for further study. In this paper, shale samples were collected from the Upper Permian Dalong Formation in the northwestern margin of the Sichuan Basin. The pore structures were investigated before and after removing SOM by the extraction with dichloromethane or trichloromethane. The primary objective is to reveal the main storage sites of SOM and its influence on shale reservoir characterization.

2. Sampling and methodology

2.1. Samples and preparation

In this study, two gray shale samples from the Upper Permian Dalong Formation were collected from Changjianggou area in the northwestern margin of the Sichuan Basin. The fresh samples were dried at 48 °C for 24 h to remove moisture. After being crushed and sieved, a size fraction of 80 and 120 mesh (180 and 120 μm) was obtained and divided into three groups, namely, A, B, and C.

H_2O_2 or NaClO treatments are commonly used methods in removing organic matter from shale. The methods not only remove the SOM and a part of kerogen, but it also changes the mineral components and destroys pores structure of the reservoir. The SOM can be effectively removed through Soxhlet-extraction preserving the pore structure of the reservoir. Therefore, the extraction with organic solvent is adopted to remove the SOM in this study. Approximately 40 g of each sample (Group B or C) was extracted for 72 h with dichloromethane and trichloromethane, respectively. The water bath temperature of dichloromethane extraction is 48 °C, and 80 °C for trichloromethane. The acquired filtrate was concentrated through rotary evaporation and was subsequently dried by nitrogen. The amount of SOM can be identified when its weight is constant in the drying box under room temperature. The extracted samples were dried at 90 °C in a vacuum for 24 h.

2.2. Experimental methods

The vitrinite reflectance (R_O) was determined on polished core samples using a 3Y-Leica DMR XP microphotometer. The instrument was calibrated using the sapphire standard ($R_O = 0.596\%$), and measurements were conducted in an oil medium using a 50×/0.85 oil lens with an optical fiber (d) of 0.6 mm. In each sample, 30–50 different vitrinite particles were randomly selected for measurements, and the average value represented the vitrinite reflectance [23].

The mineralogical composition analyses of the samples were carried out using a Bruker D8 Advance X-ray diffractometer at 40 kV and 30 mA. In a series of distinct stages, the scanning measurements were performed at a rate of 4°/min with a slit of 1 mm between 3° and 85° (2θ). The analogous mineral content was semi-quantitatively determined using peak area integration approach correlated for Lorentz Polarization [24].

The pore structure of the shale reservoir is dominated by nanometer-sized pores (i.e. micropores and mesopores). Organic matter is the main carrier of the pores, which provides the adsorption site and storage space altogether for the adsorption and free gas [18–21]. Nanometer-sized pores in low maturity shale are also the place where shale oil is stored [6]. Low-pressure N_2 adsorption is considered a standard and preferable method for surface area and pore volume measurement of porous materials [9,25]. In the modern day, CO_2 adsorption is one of the most operative methods to characterize the micropores [26,27]. Low-pressure gas adsorption has been widely used to characterize the pore structure of shale [16,18,19]. Prior the adsorption analysis, approximately 1–2 g dried samples (Groups A, B and C) were taken and degassed. Then the low-pressure N_2 and CO_2 adsorption experiments were carried out on an ASAP-2020 (Micromeritics Instruments). Supposedly the degassing treatment should not destroy the physical and chemical structure of shale [28], hence, for safety measures, a relatively low temperature (110 °C) under a vacuum condition and with longer degassing time (24 h) were adopted. Before moving the sample tube to the analysis station, the sample should be weighed again to determine the reduction. After the N_2 adsorption analysis, a second degassing (4 h) in situ was requested before CO_2 adsorption analysis.

N_2 adsorption–desorption isotherms were obtained at 77.4 K with pressure (P/P_o) ranging from 0.001 to 0.998. The adsorption branching was chosen for the calculation of surface area and pore volume [2,21]. The surface area was calculated using the BET equation [29,30]:

$$\frac{P}{V(P_o - P)} = \frac{1}{V_m C_{\mathrm{BET}}} + \frac{(C_{\mathrm{BET}} - 1)}{V_m C_{\mathrm{BET}}}\left(\frac{P}{P_o}\right) \quad (1)$$

where P is the equilibrium pressure, P_o is the saturated vapor pressure, V is the adsorbed volume, V_m is the monolayer volume, and C_{BET} is the BET constant whose value is positive. The BET surface area (S_{BET}) was calculated using the following equation [31]:

$$S_{BET} = \frac{0.001 \times V_m \times N \times A_{N_2}}{22.4} \quad (2)$$

where V_m is the monolayer volume, N is the Avogadro' number, and A_{N_2} is the atomic surface area of N_2 at 77.4 K (0.162 nm^2). The BJH model was used to characterize pore volume distribution with an effective range of 2–100 nm.

N_2 molecules are not completely entering the narrow micropores at low temperature (77.4 K) due to lack of sufficient energy [18,32]. Therefore, N_2 was replaced by CO_2 as an adsorbent for the micropores' analysis. CO_2 molecules with a cross-sectional area of 0.17 nm^2 have higher energy in ice water bath (273.1 K). The micropores' surface and pore

volume were calculated using the Dubinin-Radushkevich (D-R) equation in the pressure (P/P_o) ranging 1×10^{-5}–3.2×10^{-2} [18,27,33].

$$V_a = V_{micro} exp\left[-\left\{ \left(\frac{RT}{\beta E_o}\right) ln\frac{P_o}{P} \right\}^2 \right] \quad (3)$$

where V_a is the volume of adsorbed gas at equilibrium pressure, V_{micro} is the total micropore volume, R is the gas constant, T is the Kelvins temperature, E_o is the adsorption potential, and β is a constant. The micropore-sized distribution was determined by the density functional theory (DFT) method [17,19].

3. Results and discussions

3.1. Organic geochemistry

The organic geochemical data of the two group samples are shown in Table 1, and the comparisons of TOC content are presented in Fig. 1. The R_O values of the two original rocks are 0.72% and 0.64%, respectively. The Hydrogen index is 251 mg/g_{TOC} and 367 mg/g_{TOC}, respectively. The SOM contents of extracted samples with dichloromethane are 0.24% and 0.21%, respectively. The SOM contents of extracted samples with trichloromethane are 0.30% and 0.34%, respectively. The percentages of dichloromethane extractions to total organic matter are 9.5% and 3.6%, respectively. Meanwhile, the percentages of trichloromethane extractions are 11.9% and 5.8%, correspondingly. The evident high extraction contents of Sample 1 are related to the higher maturity.

The TOC content of extracted samples afterwards decreases. The B group of Sample 1 decreases by 0.12% with a decline of 4.8%, while Sample 2 decreases by 0.17% with a decline of 2.9%. The C group of Sample 1 decreases by 0.28% with a decline of 11.1%, while Sample 2 decreases by 0.30% with a decline of 5.12%. Both the dichloromethane and tricholoromethane can partially remove SOM in shale. More extractions obtained with trichloromethane because of its stronger polarity.

The soluble hydrocarbon content (S_1) of extracted samples decrease noticeably. The pyrolysis hydrocarbon content (S_2) and hydrogen index (I_H) also show a certain reduction. Due to the fact that the SOM content in Sample 1 is higher, the decrease of pyrolysis parameters became ever more apparent

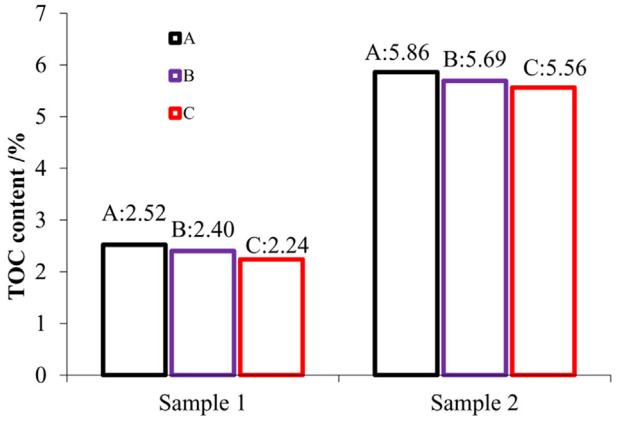

Fig. 1. Total organic carbon (TOC) content of the samples before and after extraction.

than that of Sample 2. The oxygen index of the extracted samples increases slightly. The peak temperature of pyrolysis hydrocarbon (T_{max}) is still the same, which implies that extraction does not change the significance of T_{max} as the maturity index.

3.2. Mineral composition

Accurate quantification of mineral components is still difficult. The X-ray diffraction used in this study can only be semi-quantitative [34]. The results show that the difference between mineral compositions of extracted samples with that of the original rock is insignificant and is limited within the analysis precision of X-ray diffraction (Table 2). Therefore, it can be considered that the extraction of SOM does not lead to changes in mineral compositions. The mineral compositions can be transformed into each other by oxidizing organic matter with H_2O_2 or NaClO, which would lead to the transformation

Table 2
Mineralogical compositions of the samples.

Samples	Group	Quartz/ %	Feldspar/ %	Illite-smectite/ %	Calcite/ %	Pyrite/ %	Total/ %
Sample 1	A	28.8	5.7	30.5	31.5	3.6	100
	B	27.5	6.6	31.1	31.4	3.4	100
	C	27.7	3.4	35.4	30.7	2.8	100
Sample 2	A	32	4.2	20.5	41	2.5	100
	B	31.6	4.9	18.5	43.4	1.5	100
	C	34.2	4	19.6	40.2	2	100

Table 1
Grouping and fundamental geochemical parameters of the samples.

Samples	Group	Solvent	TOC/%	R_O/%	θ/%	S_1/(mg/g)	S_2/(mg/g)	I_H/(mg/g_{TOC})	I_O/(mg/g_{TOC})	T_{max}/°C
Sample 1	A	–	2.52	0.72	–	0.55	6.32	251	5	436
	B	CH_2Cl_2	2.40	–	0.24	0.05	4.56	190	9	435
	C	$CHCL_3$	2.24	–	0.30	0.05	4.15	185	8	436
Sample 2	A	–	5.86	0.64	–	0.57	21.50	367	3	434
	B	CH_2Cl_2	5.69	–	0.21	0.08	20.48	360	4	434
	C	$CHCL_3$	5.56	–	0.34	0.06	20.23	364	4	434

R_O: vitrinite reflectance; θ: the percentage of soluble organic matter from extraction.

Table 3
Pore structure data of the samples.

Samples	Group	N_2 BET surface area/(m^2/g)	N_2 total pore volume/(cm^3/g)	N_2 mean pore size/nm	CO_2 micropore surface area/(m^2/g)	CO_2 mircopore volume/(cm^3/g)
Sample 1	A	2.61	0.0143	20.60	5.22	0.0021
	B	3.54	0.0152	17.20	6.59	0.0027
	C	4.24	0.0168	15.81	6.80	0.0027
Sample 2	A	2.84	0.0178	25.62	5.51	0.0021
	B	2.89	0.0182	25.21	6.32	0.0025
	C	3.13	0.0197	25.15	7.25	0.0029

of reservoir structure. The pore structure of shale reservoir has not changed throughout the extraction. Therefore, the difference in the analysis of the reservoir structure is vital.

3.3. Gas adsorption analysis

In comparison to the raw samples (Group A), the surface area and pore volume of the extracted samples (Groups B and C) increased in varying degree (Table 3). The SOM in shale reservoir occupies part of the pore volume. The solid state of SOM at 77.4 K reduces the pore volume occupied by the nitrogen molecules, thus, the pore volume of the extracted samples increased. The SOM presents liquid properties at 273.1 K. Although some of the carbon dioxide molecules can be dissolved in SOM, the content remains very low at relatively low-pressure and can be overlooked due to its insignificance [35]. There are two explanations for the increase of surface area. One is that SOM exists in a small throat channel and it blocks the passage of gas diffusion. The low-pressure gas molecules (N_2 or CO_2) experience difficulties entering internal pores blocked by SOM. The other is that SOM is attached directly on the surface of the porous kerogen. The more irregular surface was exposed after removing SOM. Therefore, more micropores and small mesopores could be probed by gas molecules as the surface area increases.

Observable hysteresis loops are present in the N_2 adsorption–desorption isotherms of Sample 1 (Groups A, B, and C) whose area vary with different solvents (Fig. 2a–c). The areas of hysteresis in the increasing order: Group A < Group B < Group C. The hysteresis loops of Sample 2 are not noticeable, but the fine differences between adsorption and desorption curves could be seen (Fig. 3a–c). The N_2 adsorption curves of Sample 1 show more obvious differences, while the curves of Samples 2 almost coincide only with a slight difference in the maximum adsorption (Figs. 2d and 3d). This phenomenon implies that mesopores structure of extracted Sample 1 change significantly, and the Sample 2 has not changed greatly after the extraction. The surface area data showed a similar pattern. The surface area of Sample 1 increased significantly after extraction. However, the surface

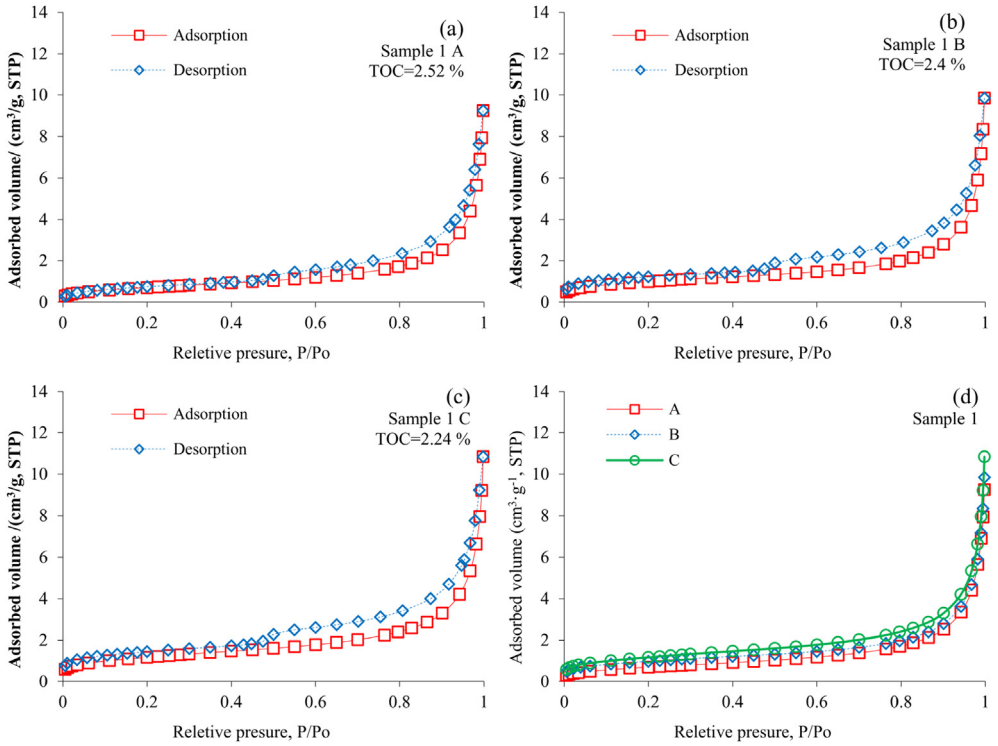

Fig. 2. Low-pressure nitrogen adsorption–desorption isotherms of Sample 1 (77.4 K).

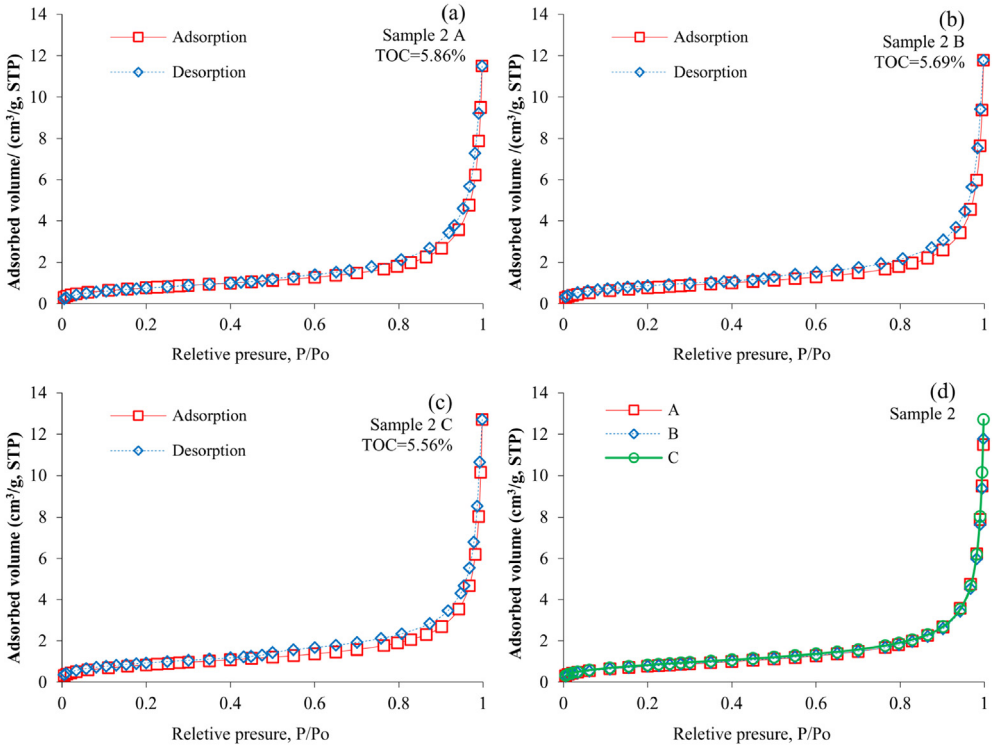

Fig. 3. Low-pressure nitrogen adsorption–desorption isotherms of Sample 2 (77.4 K).

area of Sample 2 increased minimally. The variation of the pore size is in the opposite trend with the surface area. The mean pore size of Sample 2 is larger than that of Sample 1 (Table 3).

The characteristics of mesopores are extended to the measure of micropores by CO_2 adsorption (Fig. 4). The micropores' surface area and volume of extracted samples increase in different degrees (Table 3). Compared to N_2 adsorption, CO_2 adsorption amounts of extracted Sample 2 increase greatly, which show that the extraction mainly affects micropores.

The distributions of pore volume for the studied samples are presented in Fig. 5. Comparing with the raw sample (Group A), the micropores and mesopores ranging between 2 and 20 nm in size of the extracted sample 1 (Group B and C) increase noticeable, whereas there was no significant change in larger mesopores and macropores. However, only the pores less than 5 nm in size had a varying outcome in Sample 2.

According to the results above, it can be considered that the residual SOM in shale samples occur mainly in micropores and small mesopores. This is similar to the study about SOM in coal reported by Yang et al. [15]. They concluded that the SOM in coal is mainly stored in pores between 1.7 and 5.0 nm in size. The difference between Sample 1 and Sample 2 is mainly related to maturity. Sample 1 has been in the middle level of maturity, and a large number of SOM was generated by means of cracking kerogen. Partly, SOM has been migrated and stored in the pores of organic matter and clay minerals. Whereas the maturity of Sample 2 is lower, the SOM content is less than half of the Sample 1 value. The SOM in Sample 2 is still mainly stored in smaller pores in organic matter.

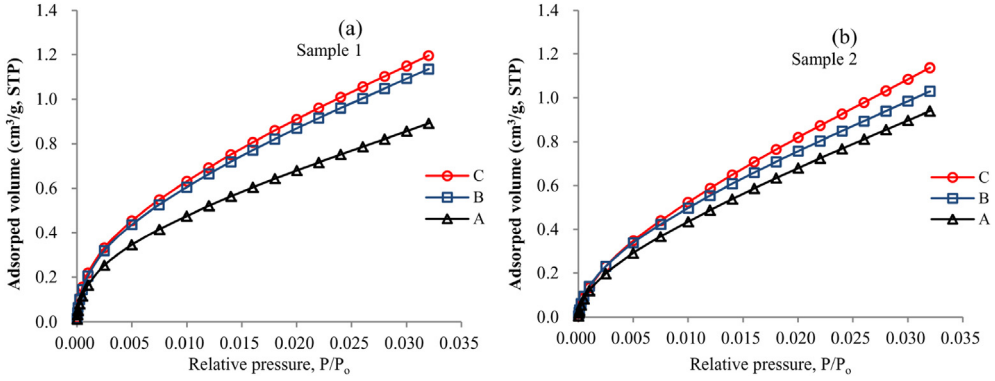

Fig. 4. CO_2 adsorption isotherms (273.1 K) of the samples.

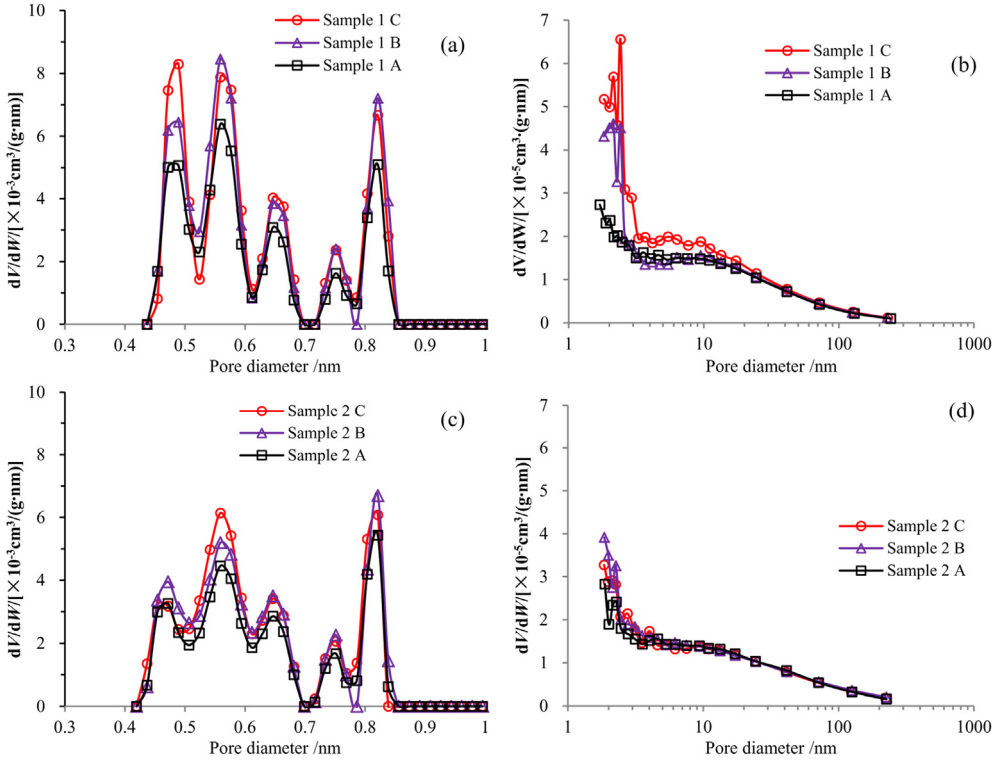

Fig. 5. Pore volume distributions of Sample 1 (a and b) and Sample 2 (c and d).

4. Conclusions

(1) The SOM in low mature shale can be effectively removed by Soxhlet extraction. Trichloromethane possesses stronger polarity which makes it better than dichloromethane for extraction. The pyrolysis parameters (e.g. TOC content, S_1, S_2, I_H) of the extracted samples declined, but the mineral composition was not altered. Thus, the original pore structure is thought to be unaffected by the extraction.

(2) The residual SOM in low mature shale has an important influence on the measurement and characterization of pore structure. The SOM inhabits pore volume, and it hinders pore connectivity. The extraction increases the surface area and pore volume of the samples greatly.

(3) The SOM occurs mainly in the micropores and small mesopores, and their occupied pore size range is influenced by the maturity. For the shale samples with lower maturity, the SOM is mainly hosted in pores with a diameter less than 5 nm. For the shale samples with moderate maturity, micropores and mesopores ranging between 2 and 20 nm are the main storage space for SOM.

Foundation items

Supported by Special Program of Chinese Academy of Science (XDB10040300); National Key Basic Research Program of China (2012CB214705); National Key Technologies R & D Program of China during the 13th Five-Year Plan Period (135TP201602); National Natural Science Foundation of China (41522302, 41321002, 41502161); GIGCAS (IS-2231).

Conflict of interest

The authors declare no conflict of interest.

References

[1] J.B. Curtis, Fractured shale-gas systems, AAPG Bull. 86 (11) (2002) 1921−1938.

[2] D. Strapoć, M. Mastalerz, A. Schimmelmann, A. Drobniak, N.R. Hasenmueller, Geochemical constraints on the origin and volume of gas in the New Albany Shale (Devonian−Mississippian), eastern Illinois Basin, AAPG Bull. 94 (11) (2010) 1713−1740.

[3] A.M. Lucier, R. Hofmann, L.T. Bryndzia, Evaluation of variable gas saturation on acoustic log data from the Haynesville Shale gas play, NW Louisiana, USA, Lead. Edge 30 (3) (2011) 300−311.

[4] Xianming Xiao, Zhiguang Song, Yanming Zhu, Hui Tian, Hongwei Yin, Summary of shale gas research in North American and revelations to shale gas exploration of Lower Paleozoic strata in China south area, J. China Coal Soc. 38 (5) (2013) 721−727.

[5] J.L. Huang, C.N. Zou, J.Z. Li, D.Z. Dong, S.J. Wang, S.Q. Wang, K.M. Cheng, Shale gas generation and potential of the Lower Cambrian Qiongzhusi Formation in the Southern Sichuan Basin, China, Pet. Explor. Dev. 39 (1) (2012) 75−81.

[6] Caineng Zou, Dazhong Dong, Shejiao Wang, Jianzhong Li, Xinjing Li, Yuman Wang, Denghua Li, Keming Cheng, Geological characteristics, formation mechanism and resource potential of shale gas in China, Pet. Explor. Dev. 37 (6) (2010) 641−653.

[7] Pei Zhao, Xianqing Li, Xiangwang Tian, Guiping Su, Mingyang Zhang, Man Guo, Zeliang Dong, Mengmeng Sun, Feiyu Wang, Study on micropore structure characteristics of Longmaxi Formation shale gas

reservoirs in the southern Sichuan Basin, Nat. Gas Geosci. 25 (6) (2014) 947−956.
[8] F.Y. Wang, J. Guan, W.P. Feng, L.Y. Bao, Evolution of overmature marine shale porosity and implication to the free gas volume, Pet. Explor. Dev. 40 (6) (2013) 819−824.
[9] H. Tian, L. Pan, X.M. Xiao, R.W.T. Wilkins, Z.P. Meng, A preliminary study on the pore characterization of Lower Silurian black shales in the Chuandong Thrust Fold Belt, southwestern China using low pressure N_2 adsorption and FE-SEM methods, Mar. Pet. Geol. 48 (2013) 8−19.
[10] Digang Liang, Tonglou Guo, Jianping Chen, Lizeng Bian, Zhe Zhao, Some progressed on studies of hydrocarbon generation and accumulation in marine sedimentary regions, Southern China (part 1): distribution of four suits of regional marine source rocks, Mar. Orig. Pet. Geol. 13 (2) (2008) 1−16.
[11] L. Pan, X.M. Xiao, H. Tian, Q. Zhou, J. Chen, T.F. Li, Q. Wei, A preliminary study on the characterization and controlling factors of porosity and pore structure of the Permian shales in Lower Yangtze region, Eastern China, Int. J. Coal Geol. 146 (2015) 68−78.
[12] Jinxiong Luo, Youbin He, Characteristics of the Permian source rocks in the Middle and Upper Yangtze Region, Nat. Gas Geosci. 25 (9) (2014) 1416−1425.
[13] J. Chen, X.M. Xiao, Evolution of nanoporosity in organic-rich shales during thermal maturation, Fuel 129 (2014) 173−181.
[14] A. Furmann, M. Mastalerz, S.C. Brassell, A. Schimmelmann, F. Picardal, Extractability of biomarkers from high- and low-vitrinite coals and its effect on the porosity of coal, Int. J. Coal Geol. 107 (2013) 141−151.
[15] Y.L. Yang, Z.H. Li, H.J. Ji, Y.J. Peng, Z. Liu, Effect of soluble organic matter in coal on its pore structure and methane sorption characteristics, J. Fuel Chem. Technol. 41 (4) (2013) 385−390.
[16] Xiancai Lu, Wenxuan Hu, Qi Fu, Deyu Miao, Guanjia Zhou, Zhihua Hong, Study of combination pattern of soluble organic matter and clay minerals in the immature source rocks in Gongying Depression, China, Sci. Geol. Sin. 34 (1) (1999) 69−77.
[17] L. Wei, M. Mastalerz, A. Schimmelmann, Y.Y. Chen, Influence of Soxhlet-extractable bitumen and oil on porosity in thermally maturing organic-rich shales, Int. J. Coal Geol. 132 (2014) 38−50.
[18] D.J.K. Ross, R.M. Bustin, The importance of shale composition and pore structure upon gas storage potential of shale gas reservoirs, Mar. Pet. Geol. 26 (2009) 916−927.
[19] M. Mastalerz, A. Schimmelmann, A. Drobniak, Y.Y. Chen, Porosity of Devonian and Mississippian New Albany Shale across a maturation gradient: insights from organic petrology, gas adsorption, and mercury intrusion, AAPG Bull. 97 (10) (2013) 1621−1643.
[20] X.J. Zhu, J.G. Cai, X.Y. Xu, Z.H. Xie, Discussion on the method for determining BET specific surface area in argillaceous source rocks, Mar. Pet. Geol. 48 (2013) 124−129.
[21] G.R. Chalmers, R.M. Bustin, I.M. Power, Characterization of gas shale pore systems by porosimetry, pycnometry, surface area, and field emission scanning electron microscopy/transmission electron microscopy image analyses: examples from the Barnett, Woodford, Haynesville, Marcellus, and Doig units, AAPG Bull. 96 (6) (2012) 1099−1119.
[22] M.E. Curtis, B.J. Cardott, C.H. Sondergeld, C.S. Rai, Development of organic porosity in the Woodford Shale with increasing thermal maturity, Int. J. Coal Geol. 103 (2012) 26−31.
[23] S.F. Dai, J.H. Zou, Y.F. Jiang, C.R. Ward, X.B. Wang, T. Li, W.F. Xue, S.D. Liu, H.M. Tian, X.H. Sun, D. Zhou, Mineralogical and geochemical compositions of the Pennsylvanian coal in the Adaohai Mine, Daqingshan Coalfield, Inner Mongolia, China: modes of occurrence and origin of diaspore, gorceixite, and ammonian illite, Int. J. Coal Geol. 94 (2012) 250−270.
[24] G.R. Chalmers, R.M. Bustin, Lower Cretaceous gas shales in northeastern British Columbia, part I: geological controls on methane sorption capacity, Bull. Can. Pet. Geol. 56 (2008) 1−21.
[25] J.J. Garrido, A. Linares-Solano, J.M. Mardn-Mardnez, M. Molina-Sabio, F. Rodriguez-Reinoso, R. Torregrosa, Use of N_2 vs. CO_2 in the characterization of activated carbons, Langmuir 3 (1) (1987) 76−81.
[26] D.J. Hubert, C.M.H. Marjo, Adsorption of CO_2 and N_2 on soil organic matter: nature of porosity, surface area, and diffusion mechanisms, Environ. Sci. Technol. 30 (2) (1996) 408−413.
[27] M.M. Dubinin, Fundamentals of the theory of adsorption in micropores of carbon adsorbents: characteristics of their adsorption properties and microporous structures, Carbon 27 (3) (1989) 457−467.
[28] J.S. Bae, S.K. Bhatia, High-pressure adsorption of methane and carbon dioxide on coal, Energy Fuels 20 (2006) 2599−2607.
[29] S. Brunauer, P.H. Emmett, E. Teller, Adsorption of gases in multimolecular layers, J. Am. Chem. Soc. 60 (2) (1938) 309−319.
[30] S.J. Gregg, K.S.W. Sing, Adsorption, Surface Area and Porosity, second ed., Academic Press, New York, 1982, pp. 1−303.
[31] K.S.W. Sing, Reporting physisorption data for gas/sold systems with special reference to the determination of surface area and porosity (Recommendations 1984), Pure Appl. Chem. 57 (4) (1985) 603−619.
[32] H. Gan, S.P. Nandi, P.L. Walker Jr., Nature of the porosity in American coals, Fuel 51 (4) (1972) 272−277.
[33] C.R. Clarkson, R.M. Bustin, Variation in micropore capacity and size distribution with composition in bituminous coal of the Western Canadian sedimentary basin, Fuel 75 (13) (1996) 1483−1498.
[34] H.M. Rietveld, Line profiles of neutron powder diffraction peaks for structure refinement, Acta Crystallogr. 22 (1967) 151−152.
[35] Qin Zhou, Hui Tian, Guihua Chen, Qiang Xu, Geological model of dissolved gas in pore water of gas shale and its controlling factors, J. China Coal Soc. 38 (5) (2013) 800−805.